Article

Numerical Analysis of a Latent Heat Storage Using Plate Heat Exchanger for Absorption System Conditions

Jesús Cerezo [1], **Fernando Lara** [2], **Rosenberg J. Romero** [1,*], **Gabriela Hernández-Luna** [1,3]
and Moisés Montiel-González [4]

1 Engineering and Applied Sciences Center Research—CIICAp, Autonomous University of Morelos State, Av. Universidad 1001, Chamilpa, Cuernavaca 62210, Mexico; jesus.cerezo@uaem.mx (J.C.); gabriela.hernandez@uaem.mx (G.H.-L.)
2 Engineering Faculty, Autonomous University of Baja California, Blvd. Benito Juarez y Calle de la Normal s/n, Insurgentes Este, Mexicali 21280, Mexico; fernando.lara.chavez@uabc.edu.mx
3 Laboratorians Technicians School, Autonomous University of Morelos State, Av. Universidad 1001, Chamilpa, Cuernavaca 62210, Mexico
4 Facultad de Ciencias Químicas e Ingeniería, Universidad Autónoma del Estado de Morelos, Av. Universidad 1001, Chamilpa, Cuernavaca 62210, Mexico; moises.montiel@uaem.mx
* Correspondence: rosenberg@uaem.mx

Abstract: The use of the phase change material (PCM) as a storage medium represents an important advance to store energy for the absorption cooling systems when solar energy is not available; however, the temperature of the storage tank is a key parameter for the adequate operation of the cooling system. This paper presents a parametric analysis of a flat and a commercial plate heat exchangers with $MgCl_2 \cdot 6H_2O$ as the PCM at absorption cooling conditions. The plate heat exchanger (PHE) is a chevron type with an angle of 45° and a plate area of 0.04 m^2. The governing equation was solved using the method of finite difference. The results showed that the corrugated plate improved the heat transfer than the flat plate; however, the flat plate obtained a higher operation time than the corrugated plate for the absorption cooling condition in the discharge process because the output temperature of the PHE was much higher than the operating conditions. Finally, the decrement of the PCM thickness and the increment of the input temperature and flowrate of the heating fluid improved the heat transfer of the PHE; however, the main thermal resistance was still in the PCM.

Keywords: phase change material; $MgCl_2 \cdot 6H_2O$; plate heat exchanger; absorption heat pump

1. Introduction

Solar energy can be used to satisfy the heat required for the absorption cooling system (ACS) sustainably. This technology mainly uses storage tanks to supply energy. Water is the common fluid used as a heating medium, which means that sensible heat (liquid phase) is only used; however, the ACS consumes great quantities of energy due to the low coefficient of performance.

The latent heat storage tank (LHST) is a feasible option to be used in absorption chillers due to the high quantity of energy accumulated in the phase change. $MgCl_2 \cdot 6H_2O$ is a good candidate for the PCM to be implemented in single-stage absorption systems because it can satisfy the operating temperature in the generator of the ACS (melting point of 117 °C). Moreover, it has good thermophysical properties and cost [1]. The use of PCM as energy storage is still limited, mainly for the low thermal conductivity process and problems with degradation composition over a very large number of cycles. These imply the reduction of heat transfer and are thus not suitable for most potential applications [2].

Corrugated plate heat exchangers could be used to improve the efficiency of the LHST [3]. Gürel, B. [4] carried out a parametric analysis in a plate heat exchanger (PHE). The parameters evaluated were the inlet temperature of the heating fluid (52, 57, and 62 °C);

steel plate thickness (0.4, 0.6, and 0.8 mm); PCMs (RT-35 Paraffin and n-octane); and the thickness of PCM distributed in one, two, and three channels of the plate heat exchanger with the same volume (0.00048 m^3). The melting temperatures of RT-35 and n-octane are 28–40 °C and 28.2 °C, respectively. The results showed that the best thermal performance obtained was with three channels, an inlet temperature of the heating fluid (HF) of 62 °C, a plate thickness of 0.6 mm, and n-octadecane. Besides Gürel, B. [5] reported that the solidification process at different inlet temperatures of the heating fluid (12, 17, and 22 °C) at similar configurations. The results showed that the solidification time of the PCM decreased by a maximum of 63% with three channels compared to a cylindrical system.

Medrano et al. [2] studied the thermal behavior during the melting and solidification stage for RT-35 paraffin, using five heat exchangers: a double pipe; a double pipe with graphite matrix; and a double-pipe with 13 radial copper fins, a finned tube, and a gasket plate and frame heat exchanger. The experimental results showed that double pipe with graphite matrix obtained the higher values of normalized powers (defined as the average thermal power by the effective area and average temperature difference) in the range of 700–800 W/m^2 K.

Lin et al. [6] evaluated the thermal performance of a pillow PHE using sodium acetate trihydrate as the PCM (melting point of 59 °C) and water as the HF. The results of the experimental test showed that the system obtained about 4.3 to 6.3 MJ from 100 to 500 L/h for the discharging test and the average power was about 2.0 to 5.0 kW.

Saeed et al. [7] experimentally evaluated a PHE made of two overlaid sheet layers, where water was used as the HF and hexadecane was used as the PCM. The results showed that this compact parallel plate showed an increment of effectiveness up to 83.1% compared with conventional storage systems, and the de optimum space between plates was 0.025 m.

Kumar et al. [8] carried out a parametric study of a SWEP B5T PHE using PureTemp 29 as the PCM (melting point of 29 °C). They concluded that the increased efficiency could be correlated to the increment of the flowrate and the temperature of the HF during the melting stage, while both parameters were not significant in the solidification stage.

Mahani et al. [9] carried out a simulation comparing a corrugated (zigzag) plate and a flat PHE using a PCM with a melting temperature close to 37 °C. It was found that the melting rate of the corrugated plate is 8% higher than the flat plate.

Wang et al. [10] carried out an experimental test and numerical model of a zigzag plate heat exchanger with a salt mixture of sodium chloride and magnesium chloride (melting point = 440 °C). The result showed that the Re and Ste numbers have a significant influence on the discharging process, while the inlet velocity has almost no impact on it.

Badenhorst [11] presented an optimization of a graphite PHE with and without phase change. The main results showed that gas and water could be used as heating fluids at high and low temperatures, respectively; however, the heating fluids had a short discharge time (about one hour). The authors concluded that the use of graphite sheets is a good option to reduce the cost.

Palomba et al. [12] carried out an experimental characterization of an asymmetric PHE and commercial paraffin as the PCM. They concluded that the heat transfer is limited when the PCM is in the solid state; besides, the efficiency in the charging process (melting) was around 83% and 95%, while the discharging process (solidification) was around 60% to 68%.

Diarce et al. [13] analyzed a flat plate heat exchanger with 15 virtual PCMs in the discharging process. The authors obtained an expression to determine the delivered power without the need for simulations as a function of the properties of the PCM and operation constraints.

Nekoonam and Ghasempour [14] studied a slab plate heat exchanger with commercial paraffin (RT50, RT65, and RT80) in a cascaded configuration. The results showed that RT80 had the highest phase change enthalpy and RT50 had the closest phase change temperature to the lower working temperature of the system.

Akyol et al. [15] studied the heat transfer in a channel with paraffin-based pure RT22H and RT25HC as PCMs. The results showed that, with the increase of 2 °C of the inlet

temperature and the decrease of 0.5 m/s of the inlet velocity, the thermal energy absorbed improved by 44%.

Cerezo et al. [3] studied a flat heat exchanger coupled an ACS and a tempering valve in TRNSYS and Equation Engineering Solver software with a sensible (water) and latent heat ($MgCl_2 \cdot 6H_2O$) storage tank. The results showed that the sensible heat storage tank is not capable to satisfy the energy demand, while the latent heat storage tank satisfies the demand with 0.50 m^3 and 50 m^2 of parabolic trough solar collector.

Most of the studies presented previously have analyzed the PCM at melting temperature around 30–45 °C, corresponding to typical domestic applications with plate heat exchangers. The use of PCM as a storage medium in absorption systems is still scarce, and the few studies found in the literature [16–19] use shell and tube heat exchangers. The objective of this paper is to analyze and compare a flat and a commercial plate heat exchanger in the charging and discharging processes at a commercial ACS condition of 11 kW of capacity using $MgCl_2 \cdot 6H_2O$ as a PCM, in which the melting point is 117 °C, with enough temperature to supply energy to the generator of the ACS.

2. Latent Heat Storage Tank Modeling

The LHST is a rectangular heat exchanger, which consists of three slabs of PCM. The HF flows in four channels to extract or supply energy (see Figure 1). T_{PCM1}, T_{PCM2}, and T_{PCM3} are the temperatures at the beginning, center, and end in the center block of the PCM, respectively. T_{PCM5} and T_{PCM6} are the temperatures on the up and bottom sides at the end of the central block of the PCM, respectively. T_{HF1} and T_{HF2} are the temperatures of the HF in the channels located in the center and the side of the heat exchanger, respectively. The insulation is placed on the bottom and upper side of the LHST. The following assumptions were made in the development of the mathematical model:

- The thermal properties of the PCM and HF are homogeneous;
- The thermophysical properties of the PCM are considered constant in the liquid, solid, and phase change;
- The phase change of the PCM is assumed to be isothermal;
- The thermal resistance of the metal wall between the plates is insignificant.
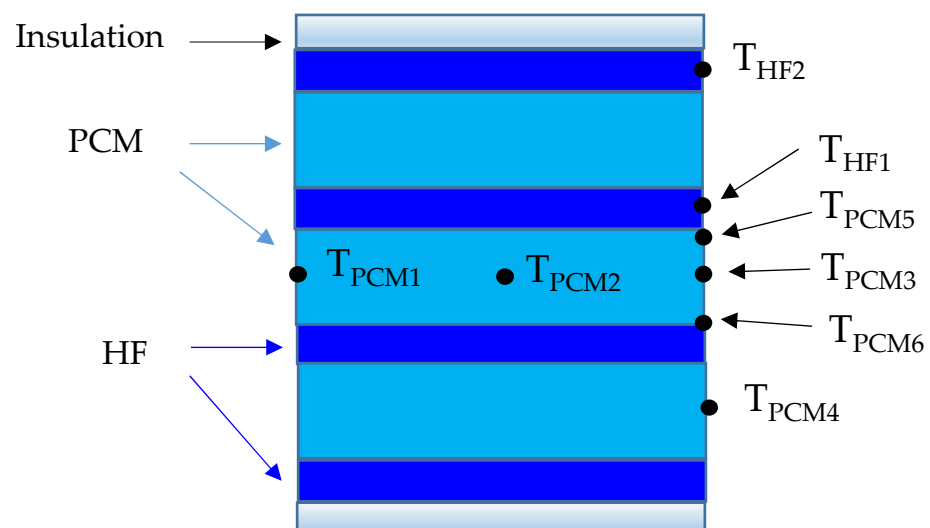

Figure 1. Schematic diagram of the LHST.

The main conservation equations governing two-dimensional transient heat transfer are presented as follows.

Heating fluid:

$$\frac{\rho_{HF} C p_{HF} V \partial T_{HF}}{\partial t} = m_{HF} C p_{HF} \partial T_{HF} - h_{HF} A_{HF} (T_{HF} - T_{PCM}), \tag{1}$$

where m, T, Cp, h, t, and ρ are the flowrate (kg/s), temperature (°C), heat capacity (kJ/kg °C), convective heat transfer coefficient (kW/m^2 °C), time (s), and density (kg/m^3), respectively. V and A are the volume (m^3) and contact area (m^2), respectively.

PCM:

$$\frac{\rho_{PCM} C p_{PCM} V \partial T_{PCM}}{\partial t} = \frac{\partial}{\partial x} \left(k_{PCM} \frac{\partial T_{PCM}}{\partial x} \right) + \frac{\partial}{\partial y} \left(k_{PCM} \frac{\partial T_{PCM}}{\partial y} \right), \tag{2}$$

where k is the thermal conductivity (kW/m^2 °C).

Insulation:

$$\frac{\rho_{ISO} C p_{ISO} V \partial T_{ISO}}{\partial t} = \frac{\partial}{\partial x} \left(k_{ISO} \frac{\partial T_{ISO}}{\partial x} \right) - U_{ISO} A_{ISO,EXT} (T_{ISO} - T_{ENV}) - h_{HF} A_{ISO,INT} (T_{ISO} - T_{HF}), \tag{3}$$

where U and V are the overall heat transfer (kW/m^2 °C) and the volume (m^3), respectively. T_{ISO} and T_{ENV} mean the temperatures of the isolating material and the environment, respectively. $A_{ISO,EXT}$ and $A_{ISO,INT}$ are the contact area in the external (environment) and internal (heating fluid) part, respectively.

The main boundary and initial conditions are presented as follows.

Insulation:

$$- k_{ISO} \frac{\partial T_{ISO}(t)}{\partial y} = h_{ENV} (T_{ISO} - T_{ENV}), \tag{4}$$

$$\frac{\partial T_{ISO}(t)}{\partial x} = 0 \tag{4b}$$

PCM (sensible heat):

$$- k_{PCM} \frac{\partial T_{PCM}(t)}{\partial y} = h_{HF} (T_{PCM} - T_{HF}), \tag{5}$$

$$\frac{\partial T_{PCM}(t)}{\partial x} = 0, \tag{5b}$$

Initial conditions:

$$T_{PCM}(t=0) = T_{ISO}(t=0) = 117 \,°C, \tag{6}$$

The liquid fraction (qu) = 0 in melting stage (charge) at t = 0, and qu =1 in solidification stage (discharge).

The partial differential equations were discretized and solved by the finite difference method; each node was solved using the implicit scheme, programmed in Engineering Equation Solver software [20]. The following equations are energy balance expressed in the finite difference formulation.

Heating fluid:

$$m_{HF} C p_{HF} \left(T^{i+1}_{m-1,n} - T^{i+1}_{m,n} \right) + m_{HF} C p_{HF} \left(T^{i+1}_{m+1, n} - T^{i+1}_{m,n} \right) + h^{i+1}_{HF} \Delta A_y \left(T^{i+1}_{m,n+1} - T^{i+1}_{m,n} \right) + h^{i+1}_{HF} \Delta A_y \left(T^{i+1}_{m,n-1} - T^{i+1}_{m,n} \right) = \frac{\rho_{HF} C p_{HF} \Delta V \left(T^{i+1}_{m,n} - T^i_{m,n} \right)}{\Delta t}, \tag{7}$$

The m and n subscripts are the node counts in the x and y directions (see Figure 2), respectively. ΔAy and ΔV are the area in the "y" direction and volume element, respectively. Δt is the step time. $T^i_{m,n}$ and $T^{i+1}_{m,n}$ are the temperatures of node m, n at times $t_i = i\Delta t$ and $t_{i+1} = (I+1) \Delta t$, respectively.
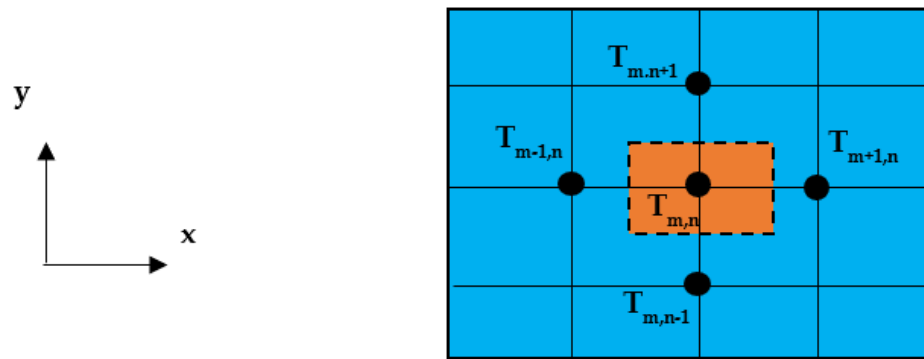
Figure 2. Schematic diagram of the volume element in the center of a node m, n of the PCM.

PCM block in the sensible heat zone:

$$\frac{k_{PCM}\Delta A_x\left(T^{i+1}_{m-1,n}-T^{i+1}_{m,n}\right)}{\Delta x} + \frac{k_{PCM}\Delta A_x\left(T^{i+1}_{m+1,n}-T^{i+1}_{m,n}\right)}{\Delta x} + \frac{k_{PCM}\Delta A_y\left(T^{i+1}_{m,n+1}-T^{i+1}_{m,n}\right)}{\Delta y} + \frac{k_{PCM}\Delta A_y\left(T^{i+1}_{m,n-1}-T^{i+1}_{m,n}\right)}{\Delta y} = \frac{\rho_{PCM}Cp_{PCM}\Delta V\left(T^{i+1}_{m,n}-T^{i}_{m,n}\right)}{\Delta t}, \tag{8}$$

PCM block in the latent heat zone:

$$\frac{k_{EFF,PCM}\Delta A_x\left(T^{i+1}_{m-1,n}-T^{i+1}_{m,n}\right)}{\Delta x} + \frac{k_{EFF,PCM}\Delta A_x\left(T^{i+1}_{m+1,n}-T^{i+1}_{m,n}\right)}{\Delta x} + \frac{k_{EFF,PCM}\Delta A_y\left(T^{i+1}_{m,n+1}-T^{i+1}_{m,n}\right)}{\Delta y} + \frac{k_{EFF,PCM}\Delta A_y\left(T^{i+1}_{m,n-1}-T^{i+1}_{m,n}\right)}{\Delta y} = \frac{\Delta Q_{LAT}}{\Delta t}, \tag{9}$$

where ΔQ_{LAT} is the sectional increment of the latent heat (kJ). Δx and Δy are the nodal points spaced throughout the rectangular mesh. k_{EFF} is the effective thermal conductivity (kW/m °C) and represents the natural convection inside an enclosure. The formulations of Equations (1)–(9) were written to rectangular coordinates based on literature by Cengel [21] and Cerezo et al. [3].

Figure 3 shows the nodal grid used in the LHST. Symmetry was considered to simplify the simulation and reduce the number of nodes by half. The longitude of the LHST was fixed "x" to 15 nodes: this means that $\Delta x = 0.022$ m. The nodes in the "y" direction are as follows: The HF process with three nodes, which means $\Delta y = 0.0015$ m. The insulation was fixed for only two nodes, which means 0.05 m (this low number of nodes was considered because the heat transfer is very low). The PCM thickness considered five nodes, which means $\Delta y = 0.0075$ m, when $th = 0.03$ m and $\Delta t = 1$ s.
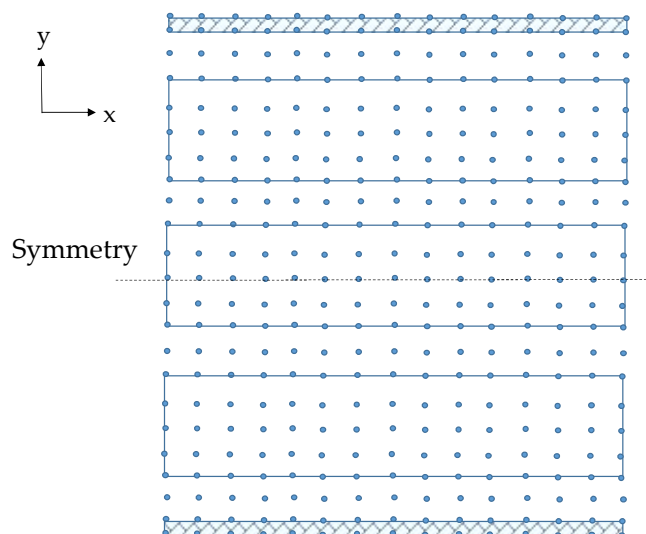

Figure 3. Schematic diagram of the nodal grid of the LHST.

Plate Heat Exchanger

The corrugated PHE is a Sondex S4 model [22]. The area and the corrugation angle are 0.04 m^2 and 60°, respectively. Some dimensions are described in Figure 4.
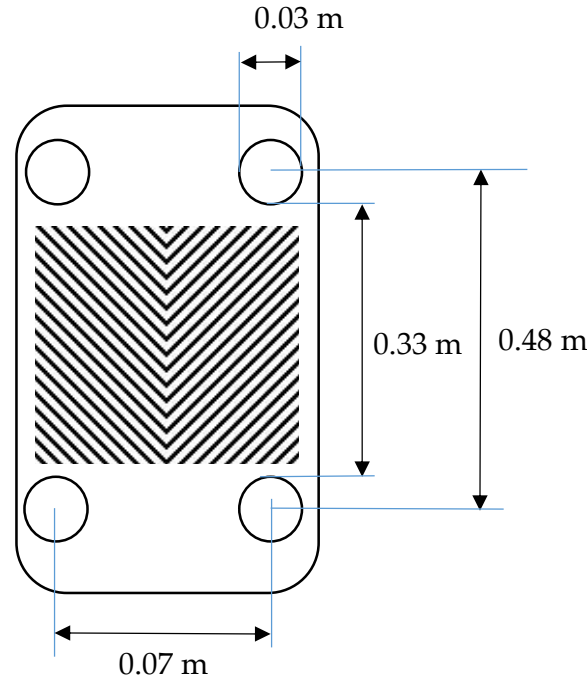

Figure 4. Characteristics of the corrugated PHE.

The Nusselt number (*Nu*) is calculated by Heavner et al. [23] for the corrugated plate at Reynolds number (*Re*) of the HF from 400 to 10,000:

$$Nu_{CORR} = 0.195 \Phi^{0.308} Re_{CORR}^{0.692} Pr_{CORR}^{1/3}, \tag{10}$$

$$Re_{CORR} = G_{CH} \frac{Dh_{CORR}}{\mu_{HF}}, \tag{11}$$

$$Dh_{CORR} = \frac{2b}{\Phi}, \tag{12}$$

where Φ is the surface enlargement factor, b is the mean channel spacing, G_{CH} is the mass velocity of the channel (kg/m^2 s), Dh is the hydraulic diameter (m), and *Pr* is the Prantl number.

The Nusselt number is obtained for short ducts and turbulent layer model for the flat plate, *Pr* > 0.5 [24–26]:

$$Nu_{FLAT} = Nu_b \left[1 + \left(\frac{Dh_{FLAT}}{L} \right)^{2/3} \right], \tag{13}$$

$$Nu_b = \frac{\left(\frac{f}{2} \right) Re_{FLAT} Pr_{FLAT}}{1 + 8.7 \left(\frac{f}{2} \right)^{\frac{1}{2}} (Pr_{FLAT} - 1)}, \tag{14}$$

$$f = (1.58 ln Re_{FLAT} - 3.28)^{-2}, \tag{15}$$

where *L* is the length of the plate heat.

Solution algorithm

The calculation procedure of the mathematical model is listed below:

1. The dimension data of the LHST is supplied, and the nodal grid is created to define Δx and Δy values (Figure 5). The initial temperatures are defined for the PCM and HF. The environment temperature is fixed at 30 °C.
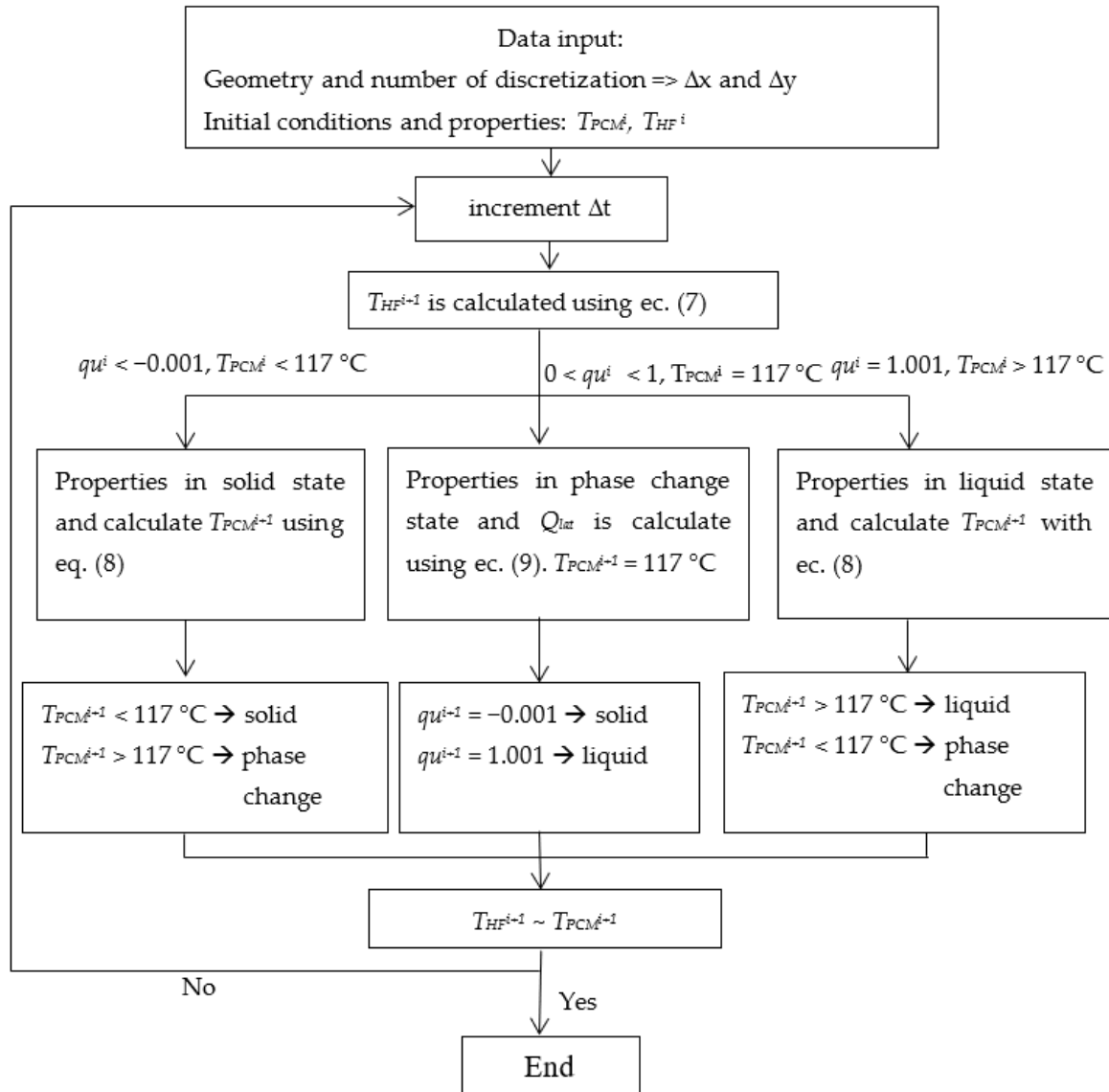

Figure 5. Algorithm for resolution of the mathematical model.

2. The increment time is supplied (Δt) and the temperatures T_{HF}^{i+1} and T_{PCM}^{i+1} are calculated simultaneously, and the thermal properties and heat transfer coefficient are calculated.

3. There are three options (solid, phase change, and liquid) for the initial data condition of the PCM. (1) The solid state should be $T_{PCM}^{i} < 117\,°C$ and $qu^{i} = -0.001$, then T_{PCM}^{i+1} is calculated with Equation (8), when $T_{PCM}^{i+1} > 117\,°C$, the phase change starts and $qu^{i+1} = 0$. (2) The phase change state should be $0 \le qu^{i} \le 1$ and $T_{PCM}^{i} = T_{PCM}^{i+1} = 117\,°C$, then Q_{lat} is calculated with Equation (9), when $qu^{i+1} = -0.001$ is in the solid state, or when $qu^{i+1} = 1.001$ is in the liquid state. (3) The liquid state should be $T_{PCM}^{i} > 117\,°C$ and $qu^{i} = 1.001$, then T_{PCM}^{i+1} is calculated with Equation (8), when $T^{i+1} < 117\,°C$, the phase change start and $qu^{i+1} = 1$.

4. When T_{HF}^{i+1} and T_{PCM}^{i+1} are similar, the program ends; otherwise, another step of time Δt is added and T_{HF}^{i+1} and T_{PCM}^{i+1} are the new values of T_{HF}^{i} and T_{PCM}^{i}.

The LHST model was validated with a PHE simulation with a similar configuration (three blocks of PCM and four channels of HF) using n-octadecane [4] in the charging process. The k_{EFF} was calculated by multiplying the thermal conductivity in the liquid phase (h_L) by a constant for this work ($k_{EFF} = k_L *$ "*cte*"). The results showed that the phase change time finished at 1000 s from the reference and 978 s proposing a "*cte*" equal to 1.3. Fan et al. [17] obtained a similar constant (1.5) using a tube and shell and hydroquinone. Another validation was carried out with $CaCl_2 \cdot 6H_2O$ as the PCM using a flat container [27]. Figure 6 shows the temperature behavior of the PCM at different effective conductivities and thicknesses (*th*). The proposing of a "*cte*" value equal to 4 is due to a maximum percent of the temperature difference between the experimental values and simulation, which was 15%. The authors use this constant because both PCMs are hexahydrate salts.
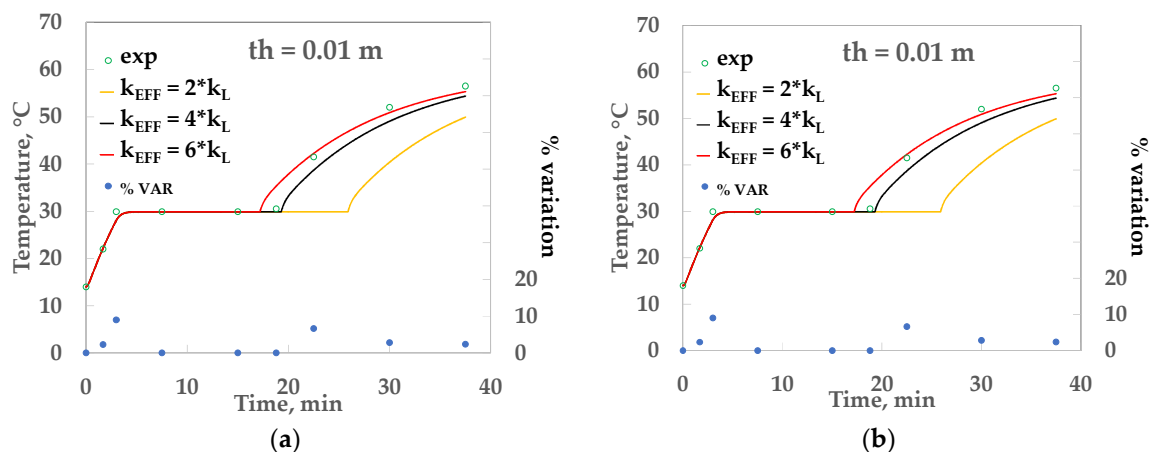

Figure 6. Validation of the mathematical model of a rectangular container at a PCM thickness of (**a**) 0.01 m and (**b**) 0.02 m.

3. Results

This section reports on the carried out thermal comparison between flat and corrugated heat plate exchangers in the charging and discharging process using a synthetic organic fluid [28] as the HF to avoid problems with vapor pressure. Table 1 shows the thermal properties of the $MgCl_2 \cdot 6H_2O$ used as the PCM.

Table 1. Thermophysical properties of the PCM [29].

Compound	Melting Temperature, °C	Heat of Fusion, kJ/kg	k, W/m °C	ρ, kg/m^3
$MgCl_2 \cdot 6H_2O$	117	168.6	0.69 (solid) at 90 °C 0.57 (liquid) at 120 °C	1569 (solid) 1450 (liquid)

3.1. Parametric Analyses in the Charging Process

The operation condition was conducted at an input temperature and flowrate of the HF at 150 °C and 0.8 kg/s, respectively; the thickness of the PCM was 0.03 m and the separation of the plates (where the HF flows) was 0.006 m.

Figures 7 and 8 show the thermal behavior in the phase change (constant temperature) and the liquid sensible heat process (increment of temperature) for a flat and corrugated PHE. Figure 7 shows the temperatures of the PCM block at the beginning, the center, and end, as shown in Figure 1. It can be seen that the latent heat process finishes at 960, 996, and 1017 s with the flat plate for T_{PCM1}, T_{PCM2}, and T_{PCM3}, respectively, while, it finishes at 765, 807, and 825 s with the corrugated plate. It is observed that the temperature difference is higher between PCM1 and PCM2 than PCM2 and PCM3 because it is higher at the beginning than the end of the LHST, and this improves the heat transfer.
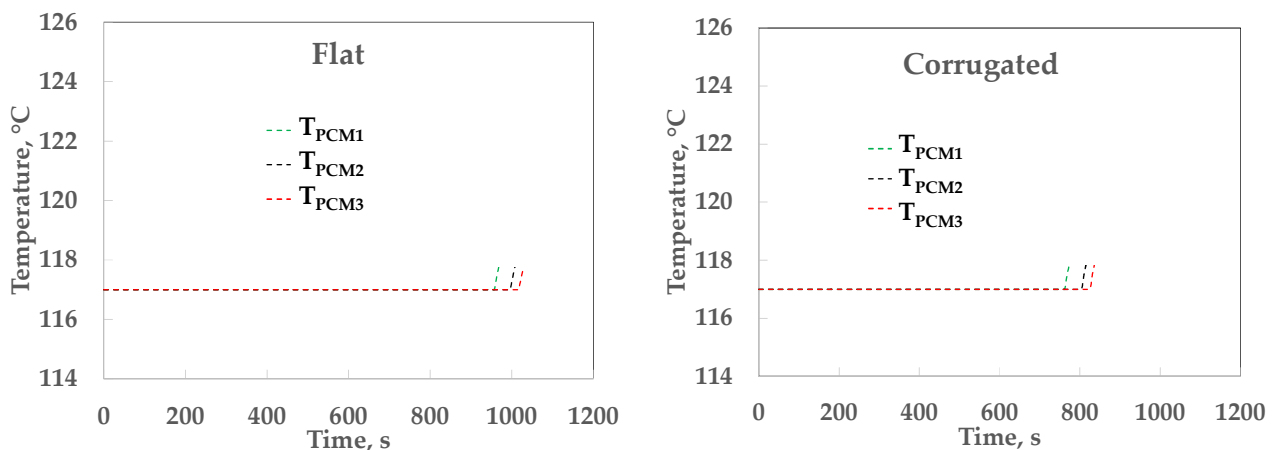
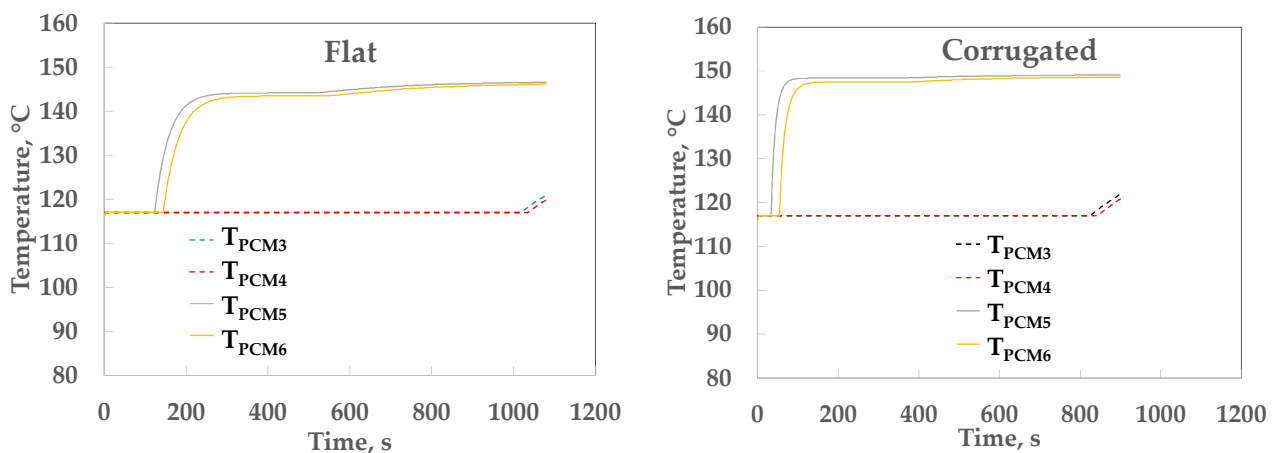**Figure 7.** Axial temperature profile in the center of the PCM.

Figure 8. Temperature profiles in the side and center of the PCM.

Figure 8 shows show that the latent heat finishes around 144 and 54 s at the contours of the central block of the PCM (T_{PCM5} and T_{PCM6}) for flat and corrugated plates, respectively, and the temperature starts to increase (liquid phase) until near 150 °C, while the latent heat lasts 1020 and 831 s in the center (T_{PCM3}) for flat and corrugated plate, respectively; besides, the latent heat process finishes first in the central block (PCM3) and then in the side blocks (PCM4). The difference time between T_{PCM3} and T_{PCM4} was 18 and 12 s for the flat and corrugated plates, respectively. This is because the PCM block in the center is heated by the HF in both faces, while the PCM block on the side is heated only in one face. After that starts the sensible heat (liquid) and the temperature starts to increase. Moreover, the latent heat process finishes first in the corrugated and then in the flat due to the higher values of the heat transfer coefficient (0.42 and 4.08 kW/m^2 °C for flat and corrugated plates, respectively).

Figure 9 shows the heat load behavior in one channel of the HF located in the center and the side (T_{HF1} and T_{HF2} from Figure 1). The heat load obtained higher values at the beginning of the LHST for both plates. The heat load in the center (Q_{CEN}) remained almost constant at a value of 3.5 kW until 117 s after that it drops for the flat plate, while the Q_{CEN} obtained a maximum value of 11.05 kW for corrugate plate after that drops similar to the flat plate. This high heat load is caused by the high temperature difference between the HT and the side PCM; however, it drops because phase change finishes in the sides of the PCM block and the temperature starts to increase, resulting in a decrement in the difference of temperature, in spite of the center in the PCM block still being in phase change (around 1000 s for flat plate and 800 s for corrugated plate). It can be seen that Q_{CEN} obtained higher

values than Q_{SIDE} because the channels placed in the center have contact with the PCM on both sides of the HF, while the channels in the sides have contact on one face for the PCM and the other face has contact with the insulation.
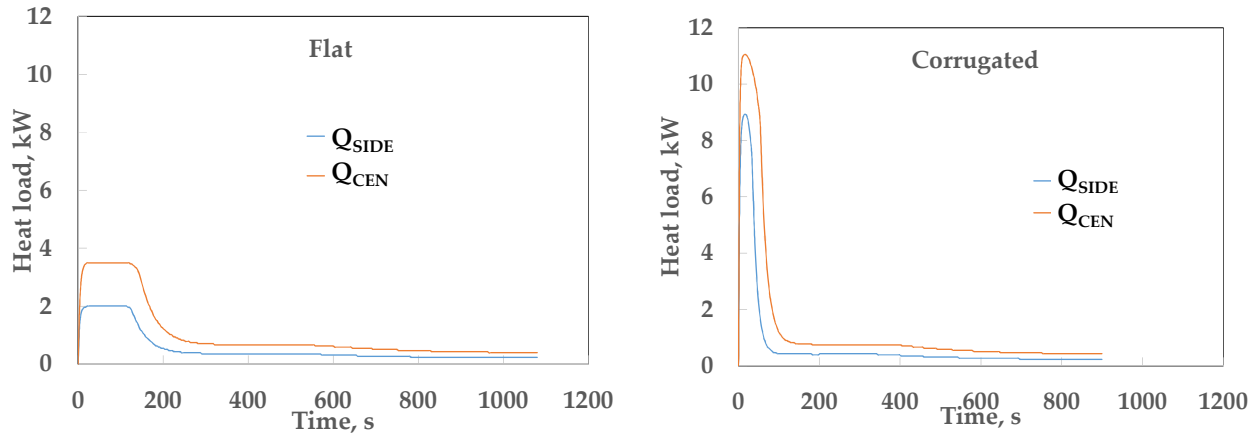

Figure 9. Heat load for the flat and corrugated LHST.

Figures 10 and 11 show the temperatures profiles in the center of the PCM at different PCM thicknesses, and the input temperature of the HF, respectively, as a function of time. Figure 10 shows that the latent heat process finishes at 520, 1020, and 1684 s for the flat plate at th = 0.02, 0.03, and 0.04 m, respectively, while it finishes at 387, 831, and 1419 s for the corrugated plate. The latent heat process takes less time for corrugated than the flat plate; besides, the phase change stage takes less time at lower PCM thicknesses.
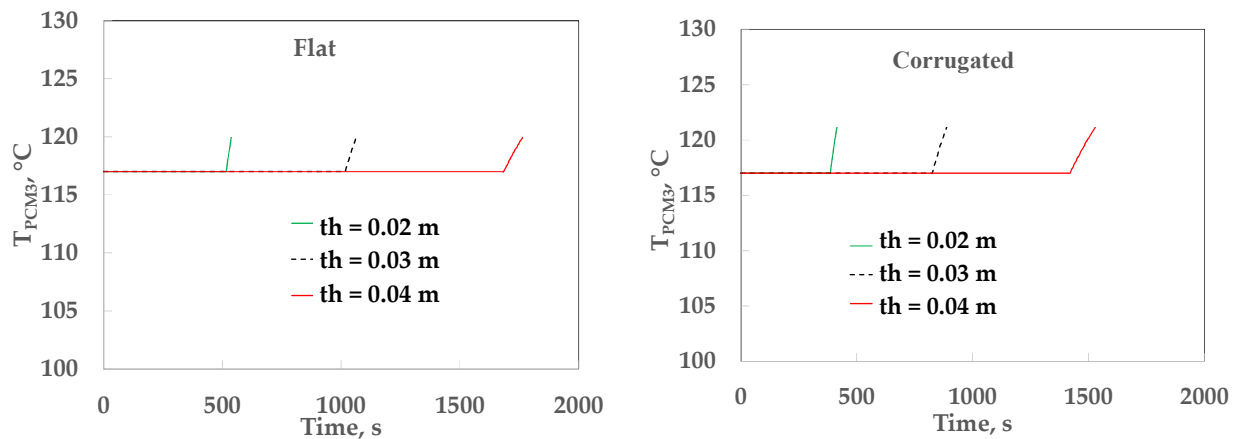
Figure 10. Temperatures profiles in the center of the PCM at different PCM thicknesses.

Figure 11 shows that when the input temperature of the HF increases, the time of the latent heat process is shorter, caused by the different temperatures between the HF and the melting point of the PCM that improve the heat transfer. The latent heat process lasts 1368 and 1104 s at $T_{HF,IN}$ = 140 °C for the flat and corrugated plate, respectively, while the phase change finishes at 1017 and 825 s at $T_{HF,IN}$ = 150 °C.
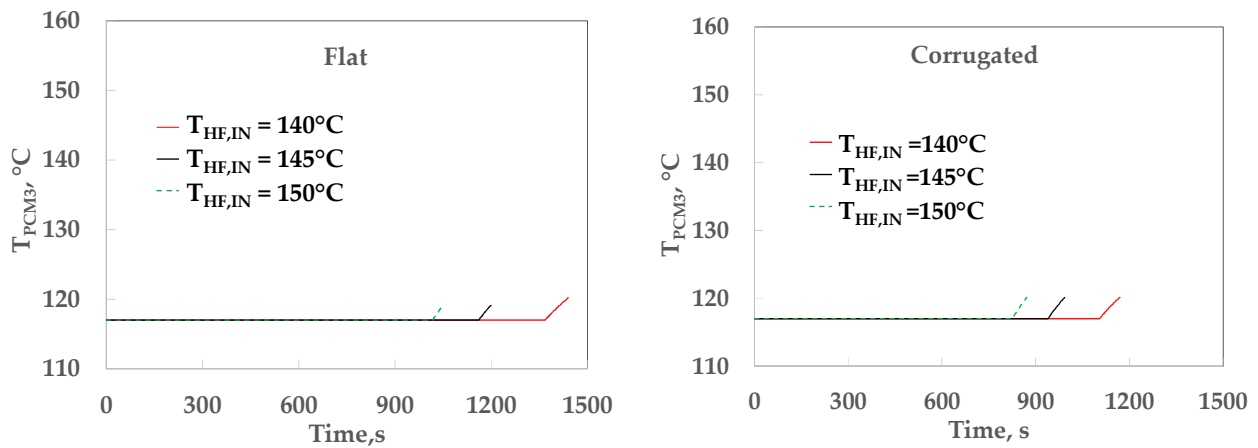
Figure 11. Temperatures profiles in the center of the PCM at different input temperatures of the HF.

3.2. Discharge Process

The operation condition of the discharging process is set by a commercial single-effect absorption chiller cooling [30]; this equipment is a very good option to significantly reduce electricity consumption as it can be thermally driven by low-grade heat sources (e.g., industrial waste heat, solar collectors, etc.). The main components are a generator, an absorber, a condenser, and an evaporator (see Figure 12), where the cooling effect takes place in the evaporator (Q_{EV}), and energy is supplied to the generator (Q_{GE}). The input and output temperatures of the generator of the ACS are 90 and 85 °C, respectively. This means that the input and output temperatures in the LHST are 85 °C and 90 °C at a flowrate of 0.8 kg/s, respectively. The initial operation condition of the PCM is 117 °C.
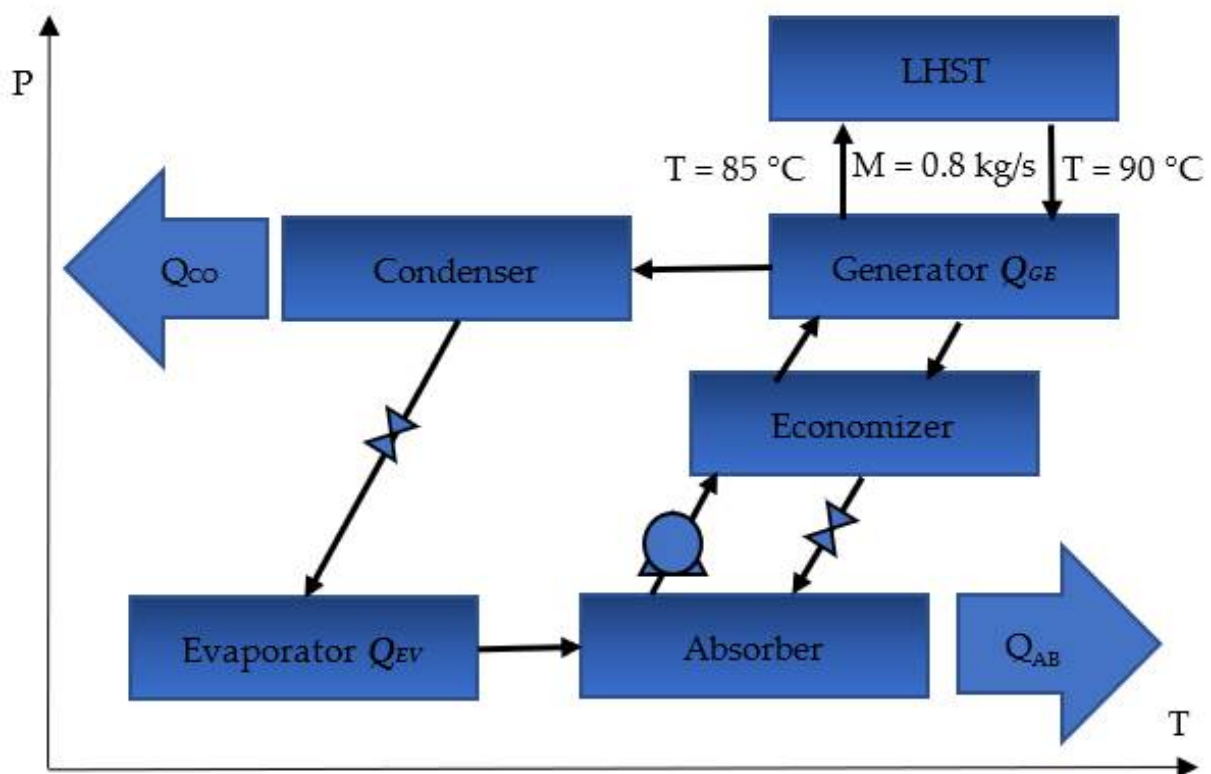

Figure 12. A schematic diagram of a single-stage absorption cycle for LiBr-H_2O.

Figure 13 shows the behavior of T_{PCM3} and $T_{HF,AVE}$ (average temperature between T_{HF1} and T_{HF2}). The $T_{HF,AVE}$ obtains a maximum value of 91.75 and 109.50 °C for the plate and corrugated plate, respectively; this high value is because the PCM in the sides is in phase change; after that, the temperature drops at lower values of 90 °C, in which the ACS can operate without an auxiliary system at 147 and 69 s for the flat and corrugated plate, respectively, in spite the temperature in the center (T_{PCM3}) is in phase change. This is due to the deficient thermal diffusivity in the PCM. The higher values of operation temperature (90 °C) represent a loss of energy because a similar coefficient of performance is obtained in the ACS at higher temperatures.
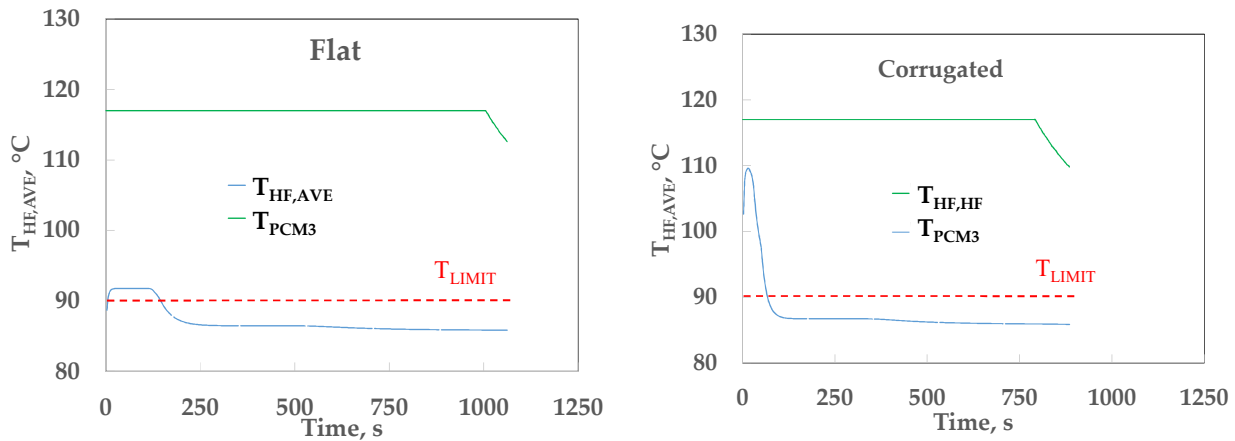

Figure 13. Outlet temperatures of the latent heat storage at different discharge temperatures at a flowrate = 0.8 kg/s.

Figure 13 showed that operation time was very short at 0.8 kg/s because of the high heat transfer of the HF; then the temperatures are much higher than the operation temperatures (90 °C), and to increase the time of operation, the total flowrate is split in half (0.4 kg/s) into two heat exchangers in a parallel arrangement. Similarly, the flowrate was split into three parts (0.27 kg/s) into three heat exchangers. Figure 14 shows that when the flowrate is reduced, the time of operation increases, and it was 285 and 420 s with the flat plate at 0.40 and 0.27 kg/s, respectively, while the corrugated plate obtained lower values of 135 and 243 s. $T_{HF,AVE}$ obtained a maximum value of 92.93 and 92.46 °C and for the flat plate at a flowrate of 0.27 and 0.40 kg/s, respectively, while $T_{HF,AVE}$ obtained 111.9 and 111.0 °C for the corrugated plate. It can be seen the temperatures are higher at a lower flowrate, because less quantity of the HF is heated. On the other hand, the $T_{HF,AVE}$ obtained higher values for the corrugated plate than for the flat plate due to the high overall heat transfer coefficient (U), as shown in Table 2.
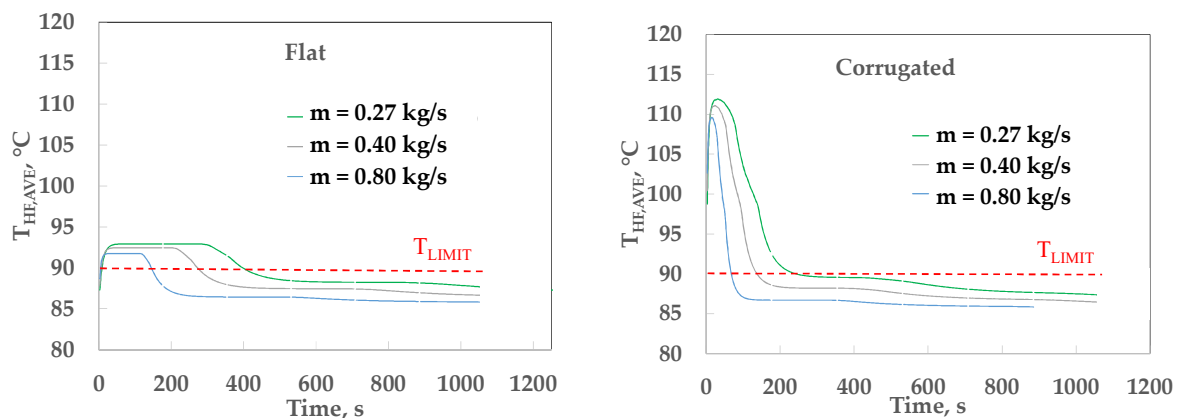

Figure 14. Outlet average temperature of the HF at different flowrates.

Table 2. Thermal resistance and overall heat transfer for the plate and corrugated plate.

	Flowrate, kg/s	R_{HF}, (m^2 C/kW)	U, (kW/m^2 C)
Flat	0.267	5.788	0.053
Flat	0.400	4.187	0.058
Flat	0.800	2.377	0.064
Corrugated	0.267	0.524	0.073
Corrugated	0.400	0.396	0.074
Corrugated	0.800	0.245	0.075

When the input temperature is lower than the limit temperature, an auxiliary system (a heater) is used to supply energy until reaching 90 °C in an ACS. $T_{HF,AVE}$ obtained values around 86 °C at 0.80 kg/s from 180 to 1000 s for the flat plate and 150 to 900 s for the corrugated plate; however, when the flowrate is 0.27 kg/s, $T_{HF,AVE}$ obtained values around 88 °C from 400 to 1000 s for the flat plate and 250 to 500 s for the corrugated plate. This indicates that the heat load of the heater will need less energy at 0.27 than 0.80 kg/s.

Table 2 shows that when the flowrate increases, the values of U increases for both the flat and corrugated plate because of the increment of the Reynold number, mainly in the corrugation plate, which produces high turbulence, the thermal resistance is low, and the time of the latent heat process is reduced; however, the increment of U is less significant for the corrugated plate than the flat plate because the thermal resistance of the PCM (13.16 m^2 °C/ kW) is not a significant value when it is compared with R_{HF}.

4. Discussion

The use of a LHST for absorption systems could be a very good advantage because they consume a great quantity of thermal energy. The actual technology still stores energy with sensible heat (water), and this becomes a bigger and heavy tank; for this study, a case in Table 3 shows a comparison of the storage energy for 1 kg of water and PCM, heated from 85 to 120 °C. The storage energy of the PCM is 1.68 times more than water, and the pressure vapor is 198 kPa, while the PCM is insignificant at 120 °C.

Table 3. Comparison of materials as storage energy.

Material	Volume, (m^3)	Vapor Pressure, (kPa)	Energy, (kJ)
Water	1.04	198	147,718
$MgCl_2 \cdot 6H_2O$	0.63	Very low	284,430

The heat load is high at the beginning of the LHST caused by the high temperature difference between the HF and the PCM block (in the sides); however, it falls when the superheating in the sides of the PCM starts, as shown in Figure 8. Some problems of the PCM are that the supercooling or superheating of the PCM must be limited because they reduce the efficiency of the PCM [31,32]; however, the results showed that the PCM presents superheating (in the charge stage) and supercooling (in the discharge stage) mainly in the sides because the heat transfer in the HF is very high. Gurel [4] and Mahani et al. [9] presented similar temperatures profiles of the PCM, with superheating in the contours using corrugated plate heat exchangers. The authors propose to reduce the superheating zone by decreasing the heat transfer of the HF and adding more channels (keeping the same PCM thickness). This will approach the thermal resistance of the HF and the PCM (13.16 m^2 °C/kW), mainly for the flat plate, as shown in Table 2 (R_{HF}). However, this is not a good option because the LHST will be much heavier and more costly.

On the other hand, the time of operation of the single-stage absorption systems is very short for this type of PHE. This is because the output temperature is very high from the minimum operation condition (90 °C). An improvement of the heat exchanger design to control the output temperature at 90 °C can be done by reducing the melting point and the thermal resistance of the PCM (using passive enhancement techniques) so that both

parameters will keep the output temperature constant due to the phase change; besides, superheating will also be reduced in the contours of the PCM.

Finally, in this study, the validation of the simulation was compared with experimental data with $CaCl_2 \cdot 6H_2O$ as the PCM. The maximum deviations between the experimental and the simulation temperatures were located at the beginning and the end of the phase change.

5. Conclusions

This paper presents a parametric analysis of a flat and a corrugated heat plate exchanger with $MgCl_2 \cdot 6H_2O$ as the PCM; the corrugated plate is a commercial heat exchanger SONDEX S4 model. The discharging process was analyzed for single-stage absorption equipment with H_2O-LiBr. The following conclusions are presented from the parametric analysis, taking a base case of a flowrate and the input temperature of the HF of 0.8 kg/s and 150 °C, respectively, a PCM thickness = 0.03 m, and a plate–plate separation of the HF = 0.003 m.

Charging process:

- The latent heat in the center (T_{PCM3}) of the PCM block lasted 1017 and 825 s for the flat and corrugated plate, respectively. The latent heat process finished first in the corrugated and then in the flat plate due to the higher value of heat transfer coefficient in the HF side.
- The latent heat process finished at 520 and 1684 s for the flat plate at PCM thickness = 0.02 and 0.04 m, respectively, while the corrugated plate took less time, and it finished at 387 and 1419 s. Higher PCM thicknesses decrease the thermal diffusivity, and the phase change process takes more time to finish.
- The increment of the input temperature of the HF from 140 to 150 °C reduced the latent heat time from 1368 to 1017 s for the flat plate and from 1104 to 825 s for the corrugated plate. A higher input temperature improves the heat transfer, caused by the differential temperature between the HF and the melting point of the PCM.

Discharging process:

- The maximum average temperature ($T_{HF,AVE}$) was 91.75 and 109.50 °C for flat and corrugated plates, respectively, at an input temperature of HF equal to 85 °C and a flowrate of 0.8 kg/s; however, the time of operation for the ACS was 147 and 69 s at 0.8 kg/s for the flat and corrugated plates, respectively, while, it took 420 and 243 s at 0.27 kg/s.
- A higher flowrate increases the overall heat transfer coefficient (U); however, it was more significant for flat plates (from 0.053 to 0.064 kW/m^2 °C) than for corrugate plates (from 0.073 to 0.075 kW/m^2 °C); this means an improvement from 17% at higher flows and 37% at lower flows for the corrugate plate.

Author Contributions: Conceptualization, J.C. and R.J.R.; methodology, F.L.; software, J.C. and M.M.-G.; validation, G.H.-L.; formal analysis, J.C., R.J.R. and F.L.; investigation, J.C.; writing—original draft preparation, J.C. and M.M.-G.; writing—review and editing, J.C., R.J.R. and F.L.; visualization, J.C. All authors have read and agreed to the published version of the manuscript.

Conflicts of Interest: The authors declare no conflict of interest.

Abbreviations

A	area: m^2
ACS	absorption cooling system
CORR	corrugated plate
Cp	heat capacity, kJ kg^{-1} °C^{-1}
FLAT	flat plate

HF	heating fluid
ISO	insulation
k	thermal conductivity, kW m^{-1} °C^{-1}
k$_{EFF}$	effective thermal conductivity, kW m^{-1} °C^{-1}
LHST	latent heat storage tank
PCM	phase change material
qu	liquid fraction
T	temperature, °C
t	time, s
th	thickness, m
U	overall heat transfer coefficient, kW m^{-2} °C^{-1}
V	volume, m^3
x	x coordinate
y	y coordinate

References

1. Choi, J.C.; Kim, S.D. Heat transfer in a latent heat-storage system using MgCl$_2$·6H$_2$O at the melting point. *Energy* **1995**, *20*, 13–25. [CrossRef]
2. Medrano, M.; Yilmaz, M.O.; Nogués, M.; Martorell, I.; Roca, J.; Cabeza, L.F. Experimental evaluation of commercial heat exchangers for use as PCM thermal storage systems. *Appl. Energy* **2009**, *86*, 2047–2055. [CrossRef]
3. Cerezo, J.; Lara, F.; Romero, R.J.; Rodríguez, A. Analysis and simulation of an absorption cooling system using a latent heat storage tank and a tempering valve. *Energies* **2021**, *14*, 1376. [CrossRef]
4. Gürel, B. A numerical investigation of the melting heat transfer characteristics of phase change materials in different plate heat exchanger (latent heat thermal energy storage) systems. *Int. J. Heat Mass Transf.* **2020**, *148*, 119117. [CrossRef]
5. Gürel, B. Thermal performance evaluation for solidification process of latent heat thermal energy storage in a corrugated plate heat exchanger. *Appl. Therm. Eng.* **2020**, *174*, 115312. [CrossRef]
6. Lin, W.; Zhang, W.; Ling, Z.; Fang, X.; Zhang, Z. Experimental study of the thermal performance of a novel plate type heat exchanger with phase change material. *Appl. Therm. Eng.* **2020**, *178*, 115630. [CrossRef]
7. Saeed, R.M.; Schlegela, J.P.; Sawafta, R.; Kalra, V. Plate type heat exchanger for thermal energy storage and load shifting using phase change material. *Energy Convers. Manag.* **2019**, *181*, 120–132. [CrossRef]
8. Kumar, N.; Chavez, R.; Banerjee, D. Experimental Validation of Thermal Performance of a Plate Heat Exchanger (PHX) with Phase Change Materials (PCM) for Thermal Energy Storage (TES). In Proceedings of the 17th IEEE Intersociety Conference on Thermal and Thermomechanical Phenomena in Electronic Systems, San Diego, CA, USA, 29 May 2018.
9. Mahani, R.B.; Mohammed, H.I.; Mahdi, J.M.; Alamshahi, F.; Ghalambaz, M.; Talebizadehsardari, P.; Yaïci, W. Phase change process in a zigzag plate latent heat storage system during melting and solidification. *Molecules* **2020**, *25*, 4643. [CrossRef]
10. Wang, P.; Li, D.; Huang, Y.; Zheng, X.; Wang, Y.; Peng, Z.; Ding, Y. Numerical study of solidification in a plate heat exchange device with a zigzag configuration containing multiple phase-change-materials. *Energies* **2016**, *9*, 394. [CrossRef]
11. Badenhorst, H. Optimising graphite composites and plate heat exchangers for latent thermal energy storage using measurements and simulation. *J. Energy Storage* **2020**, *29*, 101347. [CrossRef]
12. Palomba, V.; Brancato, V.; Frazzica, A. Thermal performance of a latent thermal energy storage for exploitation of renewables and waste heat: An experimental investigation based on an asymmetric plate heat exchanger. *Energy Convers. Manag.* **2019**, *200*, 112121. [CrossRef]
13. Diarce, G.; Campos, Á.; Sala, J.M.; García, A. A novel correlation for the direct determination of the discharging time of plate-based latent heat thermal energy storage systems. *Appl. Therm. Eng.* **2018**, *129*, 521–534. [CrossRef]
14. Nekoonam, S.; Ghasempour, R. Optimization of a solar cascaded phase change slab-plate heat exchanger thermal storage system. *J. Energy Storage* **2021**, *34*, 102005. [CrossRef]
15. Akyol, E.; Hacıhafızoğlu, O.; Susantez, Ç.; Kahveci, K.; Akyol, U. Experimental and numerical investigation of heat transfer in a channel with multiple phase change materials (PCMs). *J. Energy Storage* **2022**, *45*, 103710. [CrossRef]
16. Pintaldi, S.; Sethuvenkatraman, S.; White, S.; Rosengarten, G. Energetic evaluation of thermal energy storage options for high efficiency solar cooling systems. *Appl. Energy* **2017**, *188*, 160–177. [CrossRef]
17. Fan, Z.; Infante, C.A.; Mosaffa, A.H. Numerical modelling of high temperature latent heat thermal storage for solar application combining with double-effect H$_2$O/LiBr absorption refrigeration system. *Sol. Energy* **2014**, *110*, 398–409. [CrossRef]
18. Zhou, L.; Li, X.; Zhao, Y.; Dai, Y. Performance assessment of a single/double hybrid effect absorption cooling system driven by linear Fresnel solar collectors with latent thermal storage. *Sol. Energy* **2017**, *151*, 82–94. [CrossRef]
19. Singh, R.P.; Sze, J.Y.; Kaushik, S.C.; Rakshit, D.; Romagnoli, A. Thermal performance enhancement of eutectic PCM laden with functionalised graphene nanoplatelets for an efficient solar absorption cooling storage system. *J. Energy Storage* **2021**, *33*, 102092. [CrossRef]

20. Klein, S.A. *EES, Engineering Equation Solver; Professional Version*; FChart Software: Madison, WI, USA, 2017; Available online: http://www.fchart.com/ees/ (accessed on 16 March 2022).
21. Cengel, Y.A. *Heat and Mass Transfer: A Practical Approach*, 2nd ed.; Mc Graw-Hill Professional: New York, NY, USA, 2007.
22. Plate Heat Exchanger, Sondex S54. Available online: https://www.cjmulanixco.com/Sondex/index.php (accessed on 16 March 2022).
23. Heavner, R.L.; Kumar, H.; Wanniarachchi, A.S. Performance of an industrial plate heat exchanger: Effect of chevron angle. *AICHE Sympo. Ser.* **1993**, *89*, 262–267.
24. Kays, W.M.; Crawford, M.E. *Convective Heat and Mass Transfer*, 2nd ed.; McGraw-Hill: New York, NY, USA, 1981.
25. Kakac, S.; Yerner, Y. *Convective Heat Transfer*, 2nd ed.; CRC Press: Boca Raton, FL, USA, 1994.
26. Gnielinski, V. Forced Convection Ducts. In *Heat Exchanger Design Handbook*; Hemisphere; Begell House Inc.: New York, NY, USA, 1983; pp. 2.5.1–2.5.3.
27. Zivkovic, B.; Fujii, I. An analysis of isothermal phase change of phase change material within rectangular and cylindrical containers. *Sol. Energy* **2001**, *70*, 51–61. [CrossRef]
28. Dowthermtm Q Technical Data Sheet. Available online: https://www.dow.com/content/dam/dcc/documents/en-us/productdatasheet/176/176-01467-01-dowtherm-q-tds.pdf?iframe=true (accessed on 17 March 2022).
29. Zalba, B.; Marín, J.M.; Cabeza, L.F.; Mehling, H. Review on thermal energy storage with phase change: Materials, heat transfer analysis and applications. *Appl. Therm. Eng.* **2003**, *23*, 251–283. [CrossRef]
30. Single Effect Hot Water Absorption Chiller, Model SYDHL, SYSTEMA. Available online: https://www.systea.it/en/ (accessed on 16 March 2022).
31. Duffie, J.A.; Beckman, W.A. *Solar Engineering of Thermal Processes*, 7th ed.; John Wiley & Sons Inc.: New York, NY, USA, 1991.
32. Mofijur, M.; Mahlia, T.M.I.; Silitonga, A.S.; Ong, H.C.; Silakhori, M.; Hasan, M.H.; Putra, N.; Rahman, S.M.A. Phase change materials (PCM) for solar energy usages and storage: An overview. *Energies* **2019**, *12*, 3167. [CrossRef]